Climatic variability over the last 3000 years in the central - western Mediterranean Sea (Menorca Basin) detected by planktonic foraminifera and stable isotope records

Margaritelli G.[(1)], Cisneros M.[(2)], Cacho I.[(2)], Capotondi L.[(3)], Vallefuoco M.[(1)], Rettori R.[(4)] and Lirer F.[(1)]

1) Istituto per l'Ambiente Marino Costiero (IAMC) – Consiglio Nazionale delle Ricerche, Calata Porta di Massa, Interno Porto di Napoli, 80133, Napoli, Italy

2) GRC Geociències Marines, Dept. de Dinàmica de la Terra i de l'Oceà, Facultat de Ciències de la Terra, Universitat de Barcelona, Barcelona, Spain

3) Istituto di Scienze Marine (ISMAR), Consiglio Nazionale delle Ricerche, Via Gobetti 101, 40129 Bologna, Italy

4) Dipartimento di Fisica e Geologia – Università di Perugia, Via Alessandro Pascoli, 06123 Perugia, Italy

Corresponding author: Giulia Margaritelli (giuliamargaritelli@hotmail.it)

Abstract

The climate evolution of the last 2700 years in the central - western Mediterranean Sea has been reconstructed from marine sediment records by integrating planktonic foraminifera and geochemical signals. The results provide the characterization of six climatic phases: Balearic Bronze Age (BA), Roman Period (RP), Dark Age (DA), Medieval Climate Anomaly (MCA), Little Ice Age (LIA) and Industrial Period (IP). Paleoclimatic curve inferred from planktonic foraminifera associated with heavy values in $\delta^{18}O$ *Globigerinoides ruber* during the BA document two cold intervals (spanning ca. 200 years) related to the Homeric and Greek solar minima. The dominance of *Turborotalita quinqueloba –Globigerinita glutinata* gr. and *Globigerina bulloides* during the RP suggest high fertility surface waters condition probably triggered by the increase in precipitation. During the DA, changes in the foraminiferal paleoclimate curve and oxygen isotope values display a cold –dry phase from 700 CE to the end of the DA (ca. 850 CE). This phase corresponds to the cold Roman IV solar

minimum and marks the beginning of a long - term cooling interval that terminates during the LIA. The MCA is characterized by mild climatic conditions, interrupted at ca. 1050 CE by a cold - dry event. The gradually increase in abundance of *G. ruber* white characterize the IP warm period. The reconstructed climate evolution in the Balearic Basin results almost time - equivalent with the Mediterranean climate variability over the last 2700 years.

Keywords

Paleoclimate, Balearic Sea, fossil records, historical climate change, last three millennia.

1. Introduction

The study of last three millennia climate variability are crucial to distinguish anthropogenic from natural forcing and to provide information for medium and long - term prediction models. These reconstructions can be obtained using high-quality datasets of proxies measured from different natural archives. This background condition provides important information allowing to document considerable climate oscillations that played an important role in social reorganizations in Europe. However, our understanding of the magnitude and spatial extent as well as the possible causes and concurrences of climate changes are still limited and the scarcity of integrated information from marine records emerges (PAGES, 2009; Lionello, 2012; Luterbacher et al., 2012).

The Mediterranean area is considered one of the most responsive regions to global change and is an ideal archive to investigate paleoclimate oscillation at secular scale because of its high-sedimentation rate marine records, paleo-latitudinal and land locked configuration (e.g., Cacho et al., 1999; Rohling, 2001; Martrat et al., 2004; Frigola et al., 2007; Taricco et al., 2009; Nieto-Moreno et al., 2011; Lirer et al., 2013). Most of the current high-resolution studies are still limited to continental shelf areas (e.g., Oldfield et al., 2003; Piva et al., 2008; Lirer et al., 2014; Grauel et al., 2013; Di Bella et al., 2014; Jalali et al., 2015; Taricco et al., 2015; Bonomo et al., 2016; Margaritelli et al., 2016; Sicre et

al., 2016; Di Rita et al., 2018) and, in contrast, little is know about deep marine records (Nieto-Moreno et al., 2011; 2013a, 2013b; Cisneros et al., 2016; Gogou et al., 2016).

Planktonic Foraminifera are the most common proxy used for late Pleistocene-Holocene paleoclimatic reconstructions (e.g., Capotondi et al., 1999; Sprovieri et al., 2003; Tedesco and Thunell 2003; Amore et al., 2004; Bárcena et al., 2004; Sbaffi et al., 2004; King and Howard 2004; Hald et al., 2007; Fisler and Hendy, 2008; Piva et al., 2008; Moreno et al., 2012; Di Bella et al., 2014; Lirer et al., 2013, 2014; Munz et al., 2015; Margaritelli et al., 2016). Similarly, the oxygen isotope geochemistry of foraminifera is a well-established paleoceanographic tool (e.g., Emiliani, 1955; Shackleton, 1967) because of the oxygen in foraminiferal calcite derives from the seawater in which the organism lived. Hence, the isotope ratios can provide information about the composition and history of that water, and the environmental and climatic conditions in which the test was secreted (e.g., Capotondi et al., 1999; Schilman et al., 2001; Rohling et al., 2004; Piva et al., 2008; Nieto Moreno et al., 2011; Pearson, 2012; Grauel et al., 2013; Lirer et al., 2013, 2014; Cisneros et al., 2016).

In this work, we contribute to evidence the climate phases over the last 2700 in central-western Mediterranean (Catalan - Balearic Sea) and their link with the historical / cultural periods. We specifically address this issue by presenting an integrated study performed on planktonic foraminifera and stable isotopic record. In addition, we provide the comparison between different areas of the Mediterranean region in order to verify the synchronicity of the climate phases. This effort provide a more comprehensive picture of the climate changes in the Mediterranean region.

2. Oceanographic settings of the study area

The Balearic Sea is a sub-basin of the Western Mediterranean, located between the Iberian Peninsula and the Balearic Islands; it is commonly considered a key transition region between the Gulf of Lions and the Algerian basin (Pinot et al., 1995). The surface hydrological pattern in this area is dominated by the Modified Atlantic Water, which originates from the inflowing Atlantic Water and is progressively modified by air-sea interaction and mixing along its path through the basin (Send et al.,

1999). At the studied location, this Modified Atlantic Water arrives through the Balearic Current (Fig. 1), which flows northwards across the Balearic Sea after separating from the Northern Current that previously baths the Gulf of Lions and the Catalan coast (Montserrat et al., 2008; Lòpez-García et al., 1994). The Gulf of Lions is the region where the Western Mediterranean Deep Water forms almost each winter by deep convection offshore mostly driven by the occurrence of persistent cold, dry and persistent N-NW winds that trigger heat and buoyancy loss of offshore waters (MEDOC, 1970; Schroeder et al., 2010). In the convection process of this deep water mass also contributes the intermediate water masses, mostly Levantine Intermediate Waters formed in the Eastern Mediterranean Sea and enters into the Western Mediterranean through the Strait of Sicily (Pinardi and Masetti, 2000). Both Western Mediterranean Deep Water and particularly Levantine Intermediate Water masses form the water outflow that exits the Mediterranean through the Strait of Gibraltar (Millot, 1990; Lionello et al., 2006).

The Strait of Gibraltar plays a crucial role for the environment of the Mediterranean Sea; the fluxes through the strait compensate for the mass deficit due to the large evaporation in the basin, supply comparatively low-salinity water-masses to one of the saltiest seas on Earth, and also provide a small supply of heat, because the Mediterranean Outflow Water is cooler than the Atlantic Water inflow (i.e., Lionello, 2012; Schroeder et al., 2012; Malanotte-Rizzoli et al., 2014).

3. Material and methods

3.1 Core description and chronology

This study focus on composite multicore HER-MC-MR3.1A/3.3 recovered at 2117 m water depth in 2009 during HERMESIONE expedition on board the R/V Hespérides (for details see Cisneros et al., 2016) in the Menorca basin (Fig. 1).

The correlation between the two investigated cores HER-MC-MR3.1A and HER-MC-MR3.3, as reported in the Figure S2 of the supplementary material in Cisneros et al. (2016), is based on the occurrence of left coiled *G. truncatulinoides* bio - event dated at 1718 ± 10 year Common Era (CE)

(Lirer et al. 2013, 2014; Margaritelli et al. 2016). This bio-vent integrated with ^{210}Pb profile, AMS^{14}C, software-simulations, SST-tuning, geochemical chronostratigraphy and the top acme of *G. quadrilobatus* (Tab. 1) allowed to produce a high-resolution chronology (see for more details the Supplementary Material in Cisneros et al., 2016).

The sedimentary sequence consist on by brown - orange nannofossil and foraminiferal silty clay, slightly bioturbated with the presence of enriched layers in pteropods and gastropods fragments and some dark layers (Cisneros et al., 2016). The composite study core is 27 cm length and it was sampled at 0.5 cm resolution from top core to 15 cm below sea level and at 1 cm resolution back to the base of the core. The time interval considered in this study core spans from 702 year Before Common Era (BCE) to 1875 Common Era (CE).

3.2 Oxygen stable isotopes

Oxygen isotope analyses were performed on 15 specimens of *G. ruber* white from the size fraction > 125 µm. The measurements were performed at the geochemistry laboratory of the IAMC - CNR (Naples, Italy) with an automated continuous flow carbonate preparation Gas BenchII device (Spötl and Vennemann, 2003) and a ThermoElectron Delta Plus XP mass spectrometer. Acidification of samples was performed at 50 °C. Every 6 samples, an internal standard (Carrara Marble with δ^{18}O = −2.43 ‰ versus VPDB) was run and after 30 samples the NBS19 international standard was measured (− 2.20 ‰ VPDB). Standard deviations of oxygen isotope measures were estimated at + 0.1 ‰.

Oxygen isotope analyses on *G. bulloides* (from a size range of 250 - 355 µm) were published in Cisneros et al (2016). All the isotope data are reported in δ ‰ versus VPDB.

3.3 Planktonic foraminifera

The study of planktonic foraminiferal assemblage was made on 47 samples washed over a 63 µm sieve to remove the clay and silt fractions. Quantitative planktonic foraminiferal analyses were

carried out on the size fraction > 125 μm, considering at least 300 specimens, a number statistically consistent to perform paleoclimatic reconstructions (see Supplementary material).

Some planktonic species have been grouped as follows: *Orbulina* spp. includes both *O. universa* and *O. suturalis*; *Globigerinoides quadrilobatus* includes *G. trilobus* and *G. sacculifer*; *G. ruber* includes *G. gomitulus*; *G. bulloides* includes *G. falconensis*; *Globigerinatella siphonifera* includes *G. calida*. Analyses discriminated between left and right coiling of *G. truncatulinoides* and *G. inflata*.

The planktonic foraminiferal paleoclimate curve was constructed following Cita et al. (1977), Sanvoisin et al. (1993), Sprovieri et al., (2006) and Capotondi et al. (2016). It represents the algebraic sum of warm water species percentages (expressed as positive values) and cold water species percentages (expressed as negative values) based on ecological preferences and modern habitat characteristics reported in Hemleben et al. (1989), Rohling et al. (1993), and Pujol and Vergnaud-Grazzini (1995). Warm water species are *G. ruber* (white and pink varieties), *G. quadrilobatus*, *G. sacculifer*, *G. siphonifera* and *O. universa*. The cold - water species are *G. bulloides*, *G. glutinata*, *T. quinqueloba*, *G. inflata*, *G. truncatulinoides* left coiled and *N. pachyderma* right coiled. Negative and positive values of the curve correspond to the cold and warm surface water, respectively. In order to reconstruct paleoclimatic conditions, the relative abundance of the species or groups are plotted in percentages with respect to the total foraminiferal assemblage *vs* time. In addition, *G. glutinata* and *T. quinqueloba* are summed together (*T. quinqueloba* - *G. glutinata* gr.) as a proxy of the productivity in the sub - surface waters (Cita et al., 1977; Corselli et al., 2002; Geraga et al., 2008; Jonkers et al., 2010). *N. pachyderma* right coiled and *N. duteretrei* are summed together as a signal of cold water conditions.

Cold climate events documented in the planktonic foraminiferal paleoclimatic curve are visually compared with the chronology of solar minima events recorded in the $\Delta^{14}C$ anomalies (Stuiver et al., 1998), according to the nomenclature of Eddy (1977).

For paleoclimate reconstruction and interpretation, we adopt the ecological requirements detected by living planktonic foraminiferal distribution records (De Castro Coppa et al., 1980; Pujol and

Vergnaud Grazzini, 1995; Mallo et al., 2017) and in the Gulf of Lions sediment trap data (Rigual-Hernández et al., 2012).

4. Results

4.1 Oxygen stable isotopes

Generally, the $\delta^{18}O_{G.\ ruber}$ and $\delta^{18}O_{G.\ bulloides}$ records show a similar pattern over the last 2350 yrs; the only opposite pattern are detected at ca. 1050 CE and in the uppermost last 200 yrs (Fig. 2). In detail, $\delta^{18}O$ signals show gentle shift *vs* more positive values from base core to ca. 800 CE (Fig. 2). Only $\delta^{18}O_{G.\ bulloides}$ signal at ca. 50 CE displays a shift *vs* lower values (Fig. 2). Upwards, the $\delta^{18}O_{G.\ ruber}$ and $\delta^{18}O_{G.\ bulloides}$ signals document a long standing progressive change to higher values (from − 0.84 to + 0.85 ‰VPDB and from + 1.2 to + 1.5 ‰ VPDB, respectively) superimposed to five higher shifts centred at ca. 750 CE, 1000 CE, 1225 CE, 1500 CE and 1740 CE (Fig. 2).

4.2 Planktonic foraminifera

The planktonic foraminiferal specimens are abundant and well preserved. *G. bulloides* and *G. ruber* white variety are continuously present (mean values ca. 15 %) in the whole study interval; only from ca. 1700 CE they show a drastic reduction in percentages (Fig. 2). *G. inflata*, *G. truncatulinoides* and *Orbulina* spp. exhibit from ca. 50 CE upwards a decreasing trends followed by peaks in abundance from ca. 800 CE to top core (Fig. 2). Conversely, *T. quinqueloba* and *G. glutinata* increase from ca. 50 CE upwards reaching higher values from ca. 1750 CE to top core (Fig. 2).

G. quadrilobatus shows low abundance from base core to ca. 50 CE and becames relevant (about 9 %) at ca. 600 CE (Fig. 2). This species shows a progressive upward decreasing trend from 9% to 2% (Fig. 2). *G. ruber* pink variety shows a similar distribution pattern observed for *G. quadrilobatus* gr. (Fig. 2). *G. siphonifera* is constantly present (mean values of ca. 5 %) in the study record with an increase (mean values of ca. 10 %) in the interval from 257 BCE to 118 CE (Fig. 2) and at 882 CE (14.6 %), at 1235 CE (10.6 %), at 1357 CE (13.6 %), at 1627 CE (11.3 %) and at 1764 CE (11.6 %)

(Fig. 2). Neogloboquadrinids occur from base core to ca. 1000 CE with low values (from 1 to 9 %) (Fig. 2) and are significant at ca. 1250 CE (ca. 16 %) and from ca. 1750 CE to the top of the core (from 4 to 13 %) (Fig. 2).

5. Discussion

5.1 Paleoclimate reconstruction

The planktonic foraminiferal paleoclimate curve and stable isotopic signals were compared to document the past climate oscillations over the last 2700 yr in the Menorca basin. The principal changes observed in the studied records correspond to the historical climatic phases defined in literature, which match to the major cultural and social reorganization of the Mediterranean region with a consequent anthropogenic control on the marine ecosystems (i.e. Nieto-Moreno et al., 2011, 2013a, 2013b; Moreno et al., 2012; Lirer et al., 2013, 2014; Margaritelli et al., 2016).

Six climatic phases are defined in the records: Balearic Bronze Age (base core – 50 BCE); Roman Period (50 BCE – 500 CE); Dark Age (500 CE – 850 CE); Medieval Climate Anomaly (850 CE - 1200 CE); Little Ice Age (1200 CE – 1825 CE); Industrial Period (1825 CE – top core).

5.1.1 Balearic Bronze Age

The oldest interval is the Balearic Bronze Age which approximately corresponding to the archaeological Talayotic Period in Menorca Island and to the Iron Age in other geographic areas. Both the planktonic foraminiferal paleoclimatic and $\delta^{18}O_{G.ruber}$ curves display two cold climatic events during this period separated by a 200 yr warm phase (Fig. 2). The parallel increase in *G. bulloides* and *G. inflata* at ca. 550 BCE and at ca. 250 BCE (Fig. 2) reflects the sediment trap data of Gulf of Lions (Rigual-Hernández et al., 2012) and the living planktonic foraminiferal assemblage in the western Mediterranean Sea during winter season (De Castro Coppa et al., 1980; Pujol and Vergnaud Grazzini, 1995). In detail, the increase in abundance of *G. truncatulinoides* at 550 BCE documents winter deep mixing conditions (Pujol and Vergnaud Grazzini, 1995; Rigual-Hernández et

al., 2012), conversely the occurrence of *Neogloboquadrinids* spp. at 250 BCE, suggests lower temperature (Pujol and Vergnaud Grazzini, 1995) and a nutrient supply (Rigual-Hernández et al., 2012). These two cold events approximate the Homeric and Greek solar minima events (Eddy 1977; Stuiver et al., 1998). The climate deterioration at the time of the Greek solar minima is consistent with heavy values in $\delta^{18}O_{G.ruber}$ signal and with increase in planktonic foraminiferal cool water species (*G. scitula* and *N. pachyderma*) described in the central Tyrrhenian Sea (Margaritelli et al., 2016). In addition, this interval is equivalent in time with a cold phase between 350 and 100 BCE reported by historical source data for the central Italy (Lamb, 1977).

The 200 yr warm interval (500 - 300 BCE) is dominated by warm water indicators such as *G. ruber* (white and pink variety), *Orbulina* spp., *G. siphonifera* and *G. quadrilobatus* gr. and also relatively light values of $\delta^{18}O_{G.ruber}$ (Fig. 2). Continental records form southern Spain indicate a progressive decrease of arid conditions along the Balearic Bronze Age (Martín-Puertas et al., 2008) coincident with the description of other regions of the western Mediterranean (Piva et al., 2008; Lirer et al., 2013). The end of this Balearic Bronze climatic phase, at 50 BCE, is concomitant with the end of the Talayotic historical Period when Menorca became part of the Roman Empire from 123 BCE (De Cet et al., 2012).

5.1.2 Roman Period

The Roman Period starts with a prominent change in the planktonic foraminiferal paleoclimatic curve from warm to cooler conditions at ca. 50 BCE (Fig. 2). The Roman Period is generally characterised by three sudden cooling events (Lirer et al., 2014; Margaritelli et al., 2016). In the study core, the two strong peaks in abundance of *G. inflata*, centred at ca. 50 CE and ca. 250 CE, chronologically correspond to the cold pulses associated to Roman I and to Roman II solar minima (Fig. 2). This interpretation is supported by the occurrence of the maximum relative abundance of *G. inflata* during winter in both the sediment trap record of Gulf of Lions (Rigual-Hernández et al., 2012) and in the living planktonic foraminiferal assemblage of central - east Tyrrhenian Sea (De Castro

Coppa et al., 1980). *G. inflata* is considered a deep dwelling species (Hemleben et al., 1989; Hemleben et al., 1985) and has been used as an indicator of a cool, deep, homogenous and relatively eutrophic winter mixed layer in the Mediterranean (Rohling et al., 1995; Pérez-Folgado et al., 2003). During these two cooling events, $\delta^{18}O_{G.\ bulloides}$ signal does not show heavier values (Fig. 2), this may suggest that the intense winter mixing could be more episodic.

The paleoclimatic curve documents warm climate condition, at ca. 150 CE, between Roman I and II cold pulses. The planktonic foraminiferal assemblages during this warm phase is characterised by the increase in abundance of *G. ruber* white and *G. siphonifera* associated with *T. quinqueloba* - *G. glutinata* gr. and *G. bulloides* (Fig. 2), suggesting relatively warm climate condition during spring/fall associated with high fertility surface waters (Pujol and Vergnaud Grazzini, 1995; Rigual-Hernández et al., 2012). These conditions are in agreement with western Alboran paleoclimatic reconstruction where an increase in precipitation could produce an increase of continental river input inducing sea surface fertility (Martín-Puertas et al., 2010). In the uppermost part of the RP, the paleoclimatic curve highlights a progressive shift *vs* warm climate condition that exhibit the maximum expression at the base of the following Dark Age (Fig. 2).

5.1.3 Dark Age

The onset of Dark Age is identified at ca. 500 CE associated to a change in the paleoclimatic curve trend (Fig. 2). The paleoclimatic curve and the $\delta^{18}O_{G.\ ruber}$ signal show two distinct climatic phases (Fig. 2), in agreement with data reported in the south and central Tyrrhenian Sea (Lirer et al., 2014; Margaritelli et al., 2016). During all the DA, the $\delta^{18}O_{G.\ ruber}$ values are generally lighter and trends to higher values have been observed at the end of the period (Fig. 2).

The first one occurs between ca. 500 and ~ 700 CE and is characterized by $\delta^{18}O_{G.ruber}$ light values and the increase in abundance of *G. quadrilobatus* gr., *G. ruber* and *Orbulina* spp. (Fig. 2). These species exhibit their maximum relative abundance values during the stratification period, suggesting summer and fall climate conditions (Pujol and Vergnaud Grazzini, 1995; Rigual-Hernández et al., 2012; Mallo

et al., 2017). In contrast, the occurrence of *Neogloboquadrinids* spp. and *G. truncatulinoides* during the onset of the DA (500 - 600 CE), could suggest the intense vertical mixing during winter and the subsequent high food availability in surface waters in winter and spring lead to the proliferation of these species (Rigual-Hernández et al., 2012).

The second climate phase chronologically corresponds to the cold Roman IV solar minimum (Fig. 2). This interval is characterized by high percentages of *G. inflata* and *Neogloboquadrinids* spp., suggesting cold climate conditions during winter season (Pujol and Vergnaud Grazzini, 1995; Rigual-Hernández et al., 2012). The concomitant increase in abundance of *T. quinqueloba* - *G. glutinata* gr. (Fig. 2), suggests relatively warm climate conditions during spring/fall associated with high fertility surface waters (Rigual-Hernández et al., 2012). This feature fits with the similar micropalentological content described by Margaritelli et al. (2016) in the central Tyrrhenian Sea.

5.1.4 Medieval Climate Anomaly

The boundary between the Dark Age and Medieval Climate Anomaly is characterised by the establishment of mild climate condition documented by light values in $\delta^{18}O_{G.\ ruber}$ and $\delta^{18}O_{G.\ bulloides}$ signals (Fig. 2). This climatic signature agrees with others reconstructions performed in the Mediterranean region (i.e. Lamb, 1977; Jones et al., 2004; Mann et al., 2009; Büntgen et al., 2011; Margaritelli et al., 2016). Within this overall mild climatic conditions, at ca. 1000 - 1050 CE, the $\delta^{18}O_{G.\ ruber}$ and $\delta^{18}O_{G.\ bulloides}$ signals show a short - term cooling event [Medieval Cold Event (MCE)]. During this period, *T. quinqueloba* - *G. glutinata* gr. increase in abundance (Fig. 2), suggesting an increase in sea surface productivity (Moreno et al., 2012; Gogou et al., 2016).

In the uppermost part of the MCA (from 1150 CE to 1200 CE), high frequencies of warm waters species *G. ruber* white variety, *G. ruber* pink variety, *G. quadrilobatus* gr., *Orbulina* spp. with concomitant decrease in abundance of *T. quinqueloba* - *G. glutinata* gr., reflect warmest climate conditions during summer/fall (Rigual-Hernandez et al., 2012). This short - term warm event [Medieval Warm Event (MWE)] has been previously detected in the Tyrrhenian Sea (Lirer et al.,

2014; Margaritelli et al., 2016) suggesting that this event is almost synchronous in the western Mediterranean area.

5.1.5 Little Ice Age

The Little Ice Age starts at ca. 1200 CE and based on the $\delta^{18}O_{G.ruber}$ signal and the planktonic foraminiferal paleoclimatic curve, it results characterized by three climatic oscillations: Wolf, Spörer and Maunder cold events, as already evidenced in other sites of the Tyrrhenian Sea (Fig. 2) (Lirer et al., 2014; Margaritelli et al., 2016). All the LIA solar minima are characterized by high abundance percentages of *G. inflata* (Fig. 2) suggesting cold climate condition during winter (Rigual-Hernández et al., 2012). This species is generally considered a deep dwelling species (Hemleben et al., 1985, 1989; Rohling et al., 1995; Pérez-Folgado et al., 2003) but the positive phase relation with solar minima could support the strength of this species as a temperature signal. Moreover, these solar minima are characterized also by an increase in abundances of *G. truncatulinoides* (Fig. 2). The abundance pattern of *G. truncatulinoides* is an interesting foraminiferal signal already documented in the Tyrrhenian Sea (Lirer et al., 2013, 2014; Margaritelli et al., 2016) during the Maunder event. In the sediment trap data from Gulf of Lions, Rigual-Hernández et al. (2012) suggest that the elevated abundances of this species, during the winter–spring transition, could be indicate an affinity of this taxon with the increase mixing conditions in the Gulf of Lions. The break - down of the thermocline during winter, the vertical mixing could facilitate the ascent of *G. truncatulinoides* to the euphotic zone, where it reproduces and proliferates due to the increased primary productivity (Hemleben et al., 1985; Schiebel and Hemleben, 2005; Schiebel et al., 2002).

Margaritelli et al. (2016) linked the strong increase in abundance of *G. truncatulinoides* in the central-western Mediterranean during the Maunder to a deep water mixing induced by strong winds linked to an Atmospheric blocking event. During Maunder, a rather persisting annual mixing is also confirmed by the peak in frequency of *Orbulina* spp. (Fig. 2). In fact, this species in the sediment trap data from Gulf of Lions (Rigual-Hernández et al., 2012) displays a maximum abundance during

the summer season and as suggested by Rohling et al. (2004) and Pujol and Vergnaud-Grazzini et al., (1995) the *Orbulina* species prevail only in the summer mixed layers. In addition, the antithetic response between $\delta^{18}O_{G.\ ruber}$ and $\delta^{18}O_{G.\ bulloides}$ signals during the Maunder (Fig. 2), could suggest a possible seasonal contrast, due to strong temperature/salinity difference respectively in winter/spring and summer/autumn (Pujol and Vergnaud-Grazzini et al., 1995).

The increase in abundance of *T. quinqueloba* - *G. glutinata* gr. (Fig. 2), at the end of these solar minima events, just before the following warms phases, and the antithetic distribution of *G. inflata* and *G. truncatulinoides*, suggests relatively warm climate condition during spring/fall associated with high fertility surface waters (Rigual-Hernández et al., 2012). This higher fertility could reflect enhanced river runoff due to wetter conditions. This feature is also supported by pollen data from Tyrrhenian Sea record (Di Rita et al., 2018) where a marked increase in *Glomus*, accompanied by *Pseudischizaea*, indicating soil erosion and downwash (which is expected during a phase of general deforestation), is associated with an increase in planktonic foraminifer *T. quinqueloba*, suggesting a nutrient supply in sea surface water.

Our findings shows similar characteristics evidenced in this area from lacustrine sediment in Iberian Peninsula (Martín-Puertas et al., 2008; 2010; Moreno et al., 2012; Sánchez-López et al., 2016).

5.1.6 Industrial Period

The lower boundary of the IP in the western Mediterranean Sea corresponds to light values in $\delta^{18}O_{G.\ ruber}$ record and to an increase in abundance of warm water species *G. ruber* white variety, associated with a decrease in percentage of *G. truncatulinoides* and *G. bulloides* (Fig. 2).

These planktonic foraminiferal patterns in the Gulf of Lions sediment trap data, suggest warm climate conditions during summer (Rigual-Hernández et al., 2012). Several authors (i.e. Taricco et al., 2009; Lirer et al., 2014; Margaritelli et al., 2016) point out that this warming trend results a general signal in the central Mediterranean region.

5.2 Correlation between Mediterranean records

For the first time we provide the correlation among different regions of the Mediterranean Sea during the last 2700 years. This effort permits to verify the synchronicity of climate events in land and ocean in order to better understand global forcing within the Mediterranean region (Fig. 3).

The comparison between the marine records of Menorca basin (this study), central and south Tyrrhenian Sea (Lirer et al., 2013, 2014; Margaritelli et al. 2016), Taranto Gulf, (Grauel et al., 2013), Adriatic Sea (Piva et al., 2008), Israel (Schilman et al., 2001) and the north European continental ones (Moberg et al., 2005; Hegerl et al., 2006, 2007; Mann et al., 2008; Ljungqvist et al., 2010; Pages 2k Consortium 2013), allows to highlight a similar climate evolution at Mediterranean scale.

Notwithstanding differences in age model, we underline a general good agreement between the long and short term climate oscillations in sea surface Mediterranean $\delta^{18}O_{G.ruber}$ records (Fig. 3) during the last 2700 years.

The cooling phase at ca. 250 - 300 BCE corresponding to the Greek solar minimum is widely recognised in all the investigated Mediterranean records by $\delta^{18}O_{G.ruber}$ signatures (Fig. 3), excluding the Taranto Gulf as probably due to a regional overprint. The cooling event recorded by $\delta^{18}O_{G.ruber}$ heavy values at ca. - 600 BCE in the study core (Menorca area) has been correlated to the Homeric solar minimum (Fig. 3).

Between 220 and 800 BCE, the cold events Roman II, III and IV are well documented by $\delta^{18}O_{G.ruber}$ signals of the western basins (Fig. 3) and result time equivalent to the solar minima activity as already evidenced by Lirer et al. (2014) and Margaritelli et al. (2016) in the central Mediterranean Sea. In addition, the observed correspondence between the Roman III event with the north hemisphere continental temperature anomaly (Mann et al., 2008; and Ljungqvist et al., 2010) reveal a remarkable connection between continental and marine climatic pattern.

In the upper part of the DA, the prominent cooling event corresponding to the Roman IV solar minimum, marks the beginning of a progressive cooling trend that culminates during the LIA (Fig. 3). Trends to cool temperatures during the DA have been also reconstructed in the north Europe

continental records (PAGES 2K Consortium, 2013; McGregor et al., 2015; Büntgen et al., 2016). It results to be almost synchronous with an increase in amplitude change in solar activity ($\Delta^{14}C$, Stuiver et al., 1998) and progressive shift *vs* negative NAO index according to NAO index reconstruction of Olsen et al., (2012) (Fig. 3).

The MCA was characterized by rather temperate climate conditions as documented by marine (Schilman et al., 2001, Grauel et al., 2013; Lirer et al., 2014; McGregor et al., 2015; Cisneros et al., 2016; Margaritelli et. al., 2016) and terrestrial paleo - archives (Büntgen et al., 2016). During this time period, $\delta^{18}O_{G.ruber}$ records and foraminiferal data document mild climate conditions with a short - term cold dry event (MCE) at ca. 1050 CE and also characterized by a arboreal vegetation decrease in the central Tyrrhenian area (Moreno et al., 2012; Margaritelli et al., 2016; Di Rita et al., 2018). The MCA period was coincident with the climax of many Mediterranean cultures. During the twelfth century, the medieval Byzantine Empire goes through an important societal expansion, with substantial agricultural productivity, intensive monetary exchange, demographic growth, and its pre - eminent international political situation (Xoplaki et al., 2015).

The establishment of colder conditions in the climate system from ca. 1200 CE upwards characterized the entire LIA as provided by temperature reconstructions (PAGES 2K Consortium, 2013; Cisneros et al., 2016) and by abrupt oscillation in Mediterranean $\delta^{18}O_{G.ruber}$ records (Fig. 3). In addition, this cooling trend results almost synchronous with a progressive shift *vs* negative NAO index (Trouet et al., 2009; Olsen et al., 2012). Weak NAO index associated with Atlantic Blocking event during LIA and in particular in the late part of Maunder cold event (Barriopedro et al., 2008), has been considered by Margaritelli et al. (2016) and Di Rita et al. (2018, 2018a) as internal climate forcing to explain the changes in planktonic foraminiferal assemblage and in pollen data, respectively. In addition, Sicre et al. (2016) suggested persistent blocked regimes under a combined effect of weak NAO index with negative East Atlantic pattern (EA) in the western Mediterranean. Furthermore, Josey et al. (2011) suggest a major effect of the EA respect to the NAO in the eastern and western Mediterranean basin.

During the LIA, three distinct cooling events well documented in prominent heavy values in $\delta^{18}O_{G.\ ruber}$ signals of western and eastern Mediterranean Sea clearly resembled the Wolf, Sporer and Maunder solar minima recorded in the $\Delta^{14}C$ solar oscillation (Stuiver et al., 1998) (Fig. 3). This correlation between the $\delta^{18}O_{G.\ ruber}$ signals and solar minima supports the influence of solar forcing on the climate variability in the Mediterranean sea as already introduced in literature (Lirer et al., 2014; Margaritelli et al., 2016). In addition, as recorded in the previous cold dry event at ca. 1050 CE (MCE), a prominent decline in the forest cover in the central Tyrrhenian area is documented during the Maunder event (Di Rita et al., 2018; 2018a).

These persistent cold climate conditions are also documented in several paintings of winter landscapes showing the severe winter seasons in Europe (i.e., Brueghel 1601; Avercamp 1608) as well in the maximum frequency of freezing of Venice Lagoon occurred between 1700 and 1850 (Camuffo and Enzi, 1995).

Available data for the last two centuries are not enough to have a clear picture for this time interval, but few $\delta^{18}O_{G.ruber}$ data seem to suggest an inversion in climate *vs* warm conditions (Grauel et al., 2013; Lirer et al., 2014; Margaritelli et al., 2016).

6. Conclusions

We present a 2700 years high - resolution paleoclimate reconstruction based on planktonic foraminiferal and stable isotopic data measured on marine sediment cores from the Balearic Promontory (central-western Mediterranean).

The results allow us to identify and characterize six intervals related to known cultural / climatic phases: Balearic Bronze Age (base core –50 BCE); Roman Period (50 BCE – 500 CE); Dark Age (500 CE – 850 CE); Medieval Climate Anomaly (850 CE - 1200 CE); Little Ice Age (1200 CE – 1825 CE) and Industrial Period (1825 CE – top core). The BA is characterized by the occurrence of cold and warm water species documenting mild climate condition punctuated by two short cooling phases. This interval predates the long - term cooling trend upwards documented by planktonic foraminiferal

curve. The RP was generally dominated by the of cold winter condition with high productivity in the surface water masses. The DA shows an alternation of warm - humid and cold – warm - dry climatic oscillations. The cold - dry phase, corresponding to the solar minimum Roman IV, marks the beginning of a long - term cooling trend that terminates during the LIA. The MCA was characterized by the co - occurrence of summer and winter foraminiferal species suggesting a general mild climatic condition. This climate phase is interrupted at ca. 1050 CE by a distinct cold - dry event (MCE). During the LIA, planktonic foraminiferal assemblage and $\delta^{18}O_{G.ruber}$ signal are consistent with overall cool climate conditions documenting three short - term cooling climatic oscillations related to Wolf, Spörer and Maunder solar activity minima. In particular, the strong increase in abundance of planktonic foraminifer *G. truncatulinoides* during Maunder, documents mixing water during winter that could be related to an Atmospheric - blocking event. The warming interval during the IP is documented by the progressive increase in abundance of warm water species *G. ruber* white variety. The Mediterranean $\delta^{18}O_{G.ruber}$ framework documents remarkable similarity in the frequency of the oscillations between different parts of the Mediterranean basin, suggesting a synchronous response of marine system to past climate forcings, like the solar minima. In particular, from the DA upwards, the marine and continental proxy records show an overall parallelism suggesting a progressive cooling up to the Maunder event.

Acknowledgments

This research has been financially supported by the Project of Strategic Interest NextData PNR 2011-2013 (www.nextdataproject.it), RITMARE (www.ritmare.it), OPERA (CTM2013-48639-C2-1-R) Consolider-Redes (CTM2014-59111-REDC) and ERC-Consolidator TIMED project. Mercè Cisneros benefited from a fellowship of the University of Barcelona. This is ISMAR-CNR contribution number 1907. IC thanks ICREA Academia program from the Catalan government.

References

Amore O.F., Caffau M., Massa B., Morabito S. (2004). Late Pleistocene- Holocene paleoclimate and related paleoenvironmental changes as recorded by calcareous nannofossils and planktonic foraminifera assemblages in the southern Tyrrhenian Sea (Cape Palinuro, Italy). *Marine Micropaleontology* 52: 255–276.

Bàrcena M.A., Flores J.A., Sierro F.J., et al. (2004). Planktonic response to main oceanographic changes in the Alboran Sea (Western Mediterranean) as documented in sediment traps and surface sediments. *Marine Micropaleontology* 53: 423– 445.

Barriopedro, D., Garcìa-Herrera, R., Huth, R., 2008. Solar modulation of Northern Hemisphere winter blocking. J. Geophys. Res. 113, D14118.

Bonomo S, Cascella A, Alberico I, et al. (2016) Reworked Coccoliths as runoff proxy for the last 400 years: The case of Gaeta Gulf (central Tyrrhenian Sea, Central Italy). *Palaeogeography, Palaeoclimatology, Palaeoecology* 459: 15–28.

Büntgen U., Tegel W., Nicolussi K., et al. (2011). 2500 years of European Climate Variability and Human Susceptibility. *Science* 331: 578–82.

Büntgen U., Myglan V.S., Ljungqvist F.C., et al. (2016). Cooling and societal change during the Late Antique Little Ice Age from 536 to around 660 AD. *Nature Geoscience*. doi:10.1038/ngeo2652.

Cacho I., Pelejero C., Grimalt J.O. et al. (1999). C^{37} alkenone measurements of sea surface temperature in the Gulf of Lions (NW Mediterranean). *Organic Geochemistry* 30: 557–566.

Camuffo, D. and Enzi, S., 1995. Climatic Features during the Spörer and Maunder Minima, pp. 105-125 in: B. Frenzel (editor): "Solar Output and Climate during the Holocene", Paleoclimate Research, Special Issue 16, Fischer Verlag, Stuttgart.

Capotondi L., Borsetti A.M., Morigi C., (1999). Foraminiferal ecozones, a high resolution proxy for the late Quaternary biochronology in the Central Mediterranean Sea. *Marine Geology* 153: 253-274.

Capotondi L., Girone A., Lirer F., et al. (2016). Central Mediterranean Mid-Pleistocene paleoclimatic variability and its association with global climate. *Palaeogeography, Palaeoclimatology, Palaeoecology* 442: 72-83.

Cisneros M., Cacho I., Frigola J., et al. (2016). Sea surface temperature variability in the central-western Mediterranean Sea during the last 2700 years: a multi-proxy and multi-record approach. *Climate of the Past* 12: 849-869.

Cita M.B., Vergnaud-Grazzini C., Robert C., et al. (1977). Paleoclimatic record of a long deep sea core from the eastern Mediterranean. *Quaternary Research* 8(2): 205-235.

Corselli C., Principato M.S., Maffioli P., et al. (2002). Changes in planktonic assemblages during sapropel S5 deposition: Evidence from Urania Basin area, eastern Mediterranean. *Paleoceanography* 17(3): 1-1-1-30.

De Castro Coppa,M.G., Moncharmont Zei, M., Placella, B., Sgarrella, F., Taddei Ruggiero, E., 1980. Distribuzione stagionale e verticale dei Foraminiferi planctonici del Golfo di Napoli. Boll. Soc. Nat. Napoli 89, 1–25.

De Cet M., Gornés S., Gual J., et al. (2012). Changing settlement patterns in the Mediterranean Context: A Case Study of Menorca (Balearic Islands) from Prehistory to the 19th century AD.

CAA2012 Proceedings of the 40th Conference in Computer Applications and Quantitative Methods in Archaeology, Southampton, United Kingdom.

Di Bella L., Frezza V., Bergamin L., et al. (2014). Foraminiferal record and high resolution seismic stratigraphy of the Late Holocene succession of the submerged Ombrone River delta (Northern Tyrrenian Sea, Italy). *Quaternary International* 328-329: 287-300.

Di Rita F., Lirer F., Bonomo S., Cascella A., Ferraro, L., Florindo F., Insinga D.D., Lurcock P.C., Margaritelli G., Petrosino P., Rettori R., Vallefuoco M., Magri D., (2018). Late Holocene forest dynamics in the Gulf of Gaeta (central Mediterranean) in relation to NAO variability and human impact. *Quaternary Science Reviews*, 179, 137-152.

Di Rita, F., Fletcher, W.J., Aranbarri, J., Margaritelli, G., Lirer, F.,Magri, D. (2018a). Holocene forest dynamics in central and western Mediterranean: periodicity, spatio-temporal patterns and climate influence. *Scientific Reports*, 8:8929, DOI:10.1038/s41598-018-27056-2.

Eddy, J.A. (1977). Climate and the changing sun. *Climatic Change*, 1, 173-190.

Emiliani (1955). Pleistocene temperatures. *Journal of Geology*, 63, 538-578.

Fisler and Hendy (2008). California Current System response to late Holocene climate cooling in southern California. *Geophysical Research Letters*, VOL. 35, L09702.

Frigola J., Moreno A., Cacho I., et al. (2007). Holocene climate variability in the western Mediterranean region from a deepwater sediment record. *Paleoceanography* 22: 2209.

Geraga M., Mylona G., Tsaila-Monopoli S., et al. (2008). Northeastern Ionian Sea: palaeoceanographic variability over the last 22 ka. *Journal of Marine Systems* 74: 623–638.

Giorgi F., (2006). Climate change hot-spots. *Geophysical Research Letters* 33, Issue 8.

Gogou A., Triantaphyllou M., Xoplaki E., et al. (2016). Climate variability and socio-environmental changes in the northern Aegean (NE Mediterranean) during the last 1500 years. *Quaternary Science Reviews* 136: 209-228.

Grauel A.L., Goudeau M.L.S., de Lange G.J., et al. (2013) Climate of the past 2500 years in the Gulf of Taranto, central Mediterranean Sea: a high-resolution climate reconstruction based on $\delta^{18}O$ and $\delta^{13}C$ of *Globigerinoides ruber* (white). *The Holocene* 23, 1440–6.

Hald M., Andersson C., Ebbesen H., Jansen E., Klitgaard-Kristensen D., Risebrobakken B., Salomonsen G.R., Sarnthein M., Sejrup H.P., Telford R.J., (2007). Variations in temperature and extent of Atlantic Water in the northern North Atlantic during the Holocene. *Quaternary Science Reviews* 26(25-28), 3423-3440.

Hegerl G., Crowley T., Allen M.,et al. (2007). Detection of human influence on a new, validated, 1500 year temperature reconstruction. *Journal of Climate* 20: 650–666.

Hegerl G.C., Crowley T.J., Hyde W.T., et al. (2006). Climate sensitivity constrained by temperature reconstructions over the past seven centuries. *Nature* 440: 1029–1032.

Hemleben C., Spindler M., Beitinger I., Deuser W.G., (1985). Field and laboratory studies on the ontogeny and ecology of some globorotaliid species from the Sargasso Sea off Bermuda. *J. Foraminiferal Res.*, 14, 254 – 272.

Hemleben C., Spindler M., Anderson O.R., (1989). *Modern Planktonic Foraminifera*. Springer-Verlag, New York, 363

Jalali B., Sicre M.A., Bassetti M.A., Kallel N., (2015). Holocene climate variability in the North-western Mediterranean Sea (Gulf of Lions). Climate of the Past Discussions 11, 3187–3209.

Jones P.D., Mann M., Mann E., (2004). Climate over past millennia. *Reviews of Geophysics* 42: RG2002.

Jonkers L., Brummer G.J.A., Peeters F.J.C., et al. (2010). Seasonal stratification, shell flux, and oxygen isotope dynamics of left-coiling *N. pachyderma* and *T. quinqueloba* in the western subpolar North Atlantic. *Paleoceanography* 25: PA2204.

Josey, S.A., Somot, S., Tsimplis, M. (2011). Impacts of atmospheric modes of variability on Mediterranean Sea surface heat exchange. *Journal of Geophysical Research*, 116, C02032, doi:10.1029/2010JC006685.

King A.L., Howard W.R., 2004. *Global biogeochemical cycles*.

Lamb H.H., (1977). *Climate: Present, Past and Future*, Vol. 2. London, Methuen & Co.

Ljungqvist F.C., (2010). A new reconstruction of temperature variability in the extra-tropical Northern Hemisphere during the last two millennia. *Geografiska annaler series a-physical geography* 92A: 339–351.

Lionello P., (2012). The Climate of the Mediterranean Region: From the Past to the Future. E. Science, Burlington, MA.

Lionello, P., Malanotte-Rizzoli, R., Boscolo, R., Alpert, P., Artale, V., Li, L., Luterbacher, J., May, W., Trigo, R., Tsimplis, M., Ulbrich, U., Xoplaki, E., 2006. The Mediterranean climate: An overview of the main characteristics and issues, in: Mediterranean Climate Variability (MedClivar), Elsevier, Amsterdam, 1–26.

Lirer F., Sprovieri M., Ferraro L., et al. (2013). Integrated stratigraphy for the Late Quaternary in the eastern Tyrrhenian Sea. *Quaternary International* 292: 71– 85.

Lirer F., Sprovieri M., Vallefuoco M., et al. (2014). Planktonic foraminifera as bio-indicators for monitoring the climatic changes that have occurred over the past 2000 years in the southeastern Tyrrhenian Sea. *Integrative Zoology* 9: 542–554.

López García, M. J., Millot, C., Font, J., & García-Ladona, E. (1994). Surface circulation variability in the Balearic Basin. Journal of Geophysical Research, 99(C2), 3285–3296.

Luterbacher J., García-Herrera R., Akcer-On A., et al. (2012). A review of 2000 years of paleoclimatic evidence in the Mediterranean. In: The Climate of the Mediterranean Region: From the Past to the Future [P. Lionello (ed.)]. Elsevier, Philadelphia, PA, USA, pp. 87–185.

Malanotte-Rizzoli P., Artale V., Borzelli-Eusebi G.L., et al. (2014). Physical forcing and physical/biochemical variability of the Mediterranean Sea: a review of unresolved issues and directions for future research. *Ocean Science* 10: 281–322.

Mallo M., Ziveri P., Mortyn P.G., Schiebel R., Grelaud M. (2017). Low planktic foraminiferal diversity and abundance observed in a spring 2013 west–east Mediterranean Sea plankton tow transect. Biogeosciences, 14, 2245–2266.

Mann, M.E., Zhang, Z., Hughes, M.K., Bradley, R.S., Miller, S.K., Rutherford, S., (2008). Proxy-Based Reconstructions of Hemispheric and Global Surface Temperature Variations over the Past Two Millennia, Proc. Natl. Acad. Sci., 105, 13252-13257.

Mann M.E., Zhang Z., Rutherford S., Bradley R.S., Hughes M.K., Shindell D., Ammann C., Faluvegi G., Ni F., (2009). Global signatures and dynamical origins of the Little Ice Age and Medieval Climate Anomaly. *Science* 326, 1256–1260.

Margaritelli G., Vallefuoco M., Di Rita F., et al. (2016). Marine response to climate changes during the last four millennia in the central Mediterranean Sea. *Global and Planetary Change* 142: 53–72.

Martín-Puertas C., Valero-Garcés B.L., Brauer A., et al. (2008). The Iberian–Roman Humid Period (2600–1600 cal yr BP) in the Zoñar Lake varve record (Andalucía, Southern Spain). Quaternary Research 71, 108–120.

Martín-Puertas C., Jimenez-Espejo F., Martínez-Ruiz F., et al. (2010). Late Holocene climate variability in the southwestern Mediterranean region: an integrated marine and terrestrial geochemical approach. *Climate of the Past* 6: 807–816.

Martrat B., Grimalt J.O., López-martínez C., et al (2004). Abrupt Temperature Changes in the Western Mediterranean over the Past 250, 000 Years. *Science* 80: 306(1762).

McGregor H.V., Evans M.N., Goosse H., et al (2015). Robust global ocean cooling trend for the pre-industrial Common Era. *Nature Geoscience* 8: 671–677.

MEDOC, G. 1970: Observation of formation of Deep Water in the Mediterranean Sea, Nature 227, 1037–1040.

Millot, C. A., 1990. The Gulf of Lions' hydrodynamic. Cont. Shelf Res. 10, 885-894.

Moberg A, Sonechkin DM, Holmgren K, Datsenko NM, Karlén W (2005) Highly variable northern hemisphere temperatures reconstructed from low-and high-resolution proxy data. Nature 433(7026):613–617.

Monserrat, S., López-Jurado, J. L., & Marcos, M. (2008). A mesoscale index to describe the regional circulation around the Balearic Islands. Journal of Marine Systems, 71(3–4), 413.

Moreno A., Pérez A., Frigola J., et al (2012). The Medieval Climate Anomaly in the Iberian Peninsula reconstructed from marine and lake records. *Quaternary Science Reviews* 43: 16–32.

Munz P., Siccha M., Lückge A., Böll A., Kucera M., Schulz H., (2015). Decadal-resolution record of winter monsoon intensity over the last two millennia from planktic foraminiferal assemblages in the northeastern Arabian Sea. *The Holocene* 25(11), 1756-1771.

Nieto-Moreno V., Martínez-Ruiz F., Giralt S., et al (2011). Tracking climate variability in the western Mediterranean during the Late Holocene: a multiproxy approach. *Climate of the Past* 7: 1395–1414.

Nieto-Moreno V., Martínez-Ruiz F., Willmott V., et al (2013a). Climate conditions in the westernmost Mediterranean over the last two millennia: An integrated biomarker approach. *Organic Geochemistry* 55: 1–10.

Nieto-Moreno V., Martínez-Ruiz F., Giralt S., et al (2013b). Climate imprints during the 'Medieval Climate Anomaly' and the 'Little Ice Age' in marine records from the Alboran Sea basin. *The Holocene* 23: 1227-1237.

Oldfield TEE, Smith RJ, Harrop SR et al (2003) Field sports and conservation in the United Kingdom. *Nature* 423: 531–533.

Olsen J., Anderson N.J., Knudsen M.F., (2012). Variability of the North Atlantic Oscillation over the past 5200 years. *Nature Geosciences* 5, 808–812.

PAGES 2009. Science Plan and Implementation Strategy, IGBP Report No. 57, IGBP Secretariat, Stockholm.

PAGES 2K Consortium, 2013. Continental-scale temperature variability during the past two millennia, Nature, 6, 339–346.

Pearson, P.N. (2012). Oxygen Isotopes in Foraminifera: overview and historical review. *The Paleontological Society Papers*, Volume 18, Linda C. Ivany and Brian T. Huber (eds.), 1–38

Pérez-Folgado, M. et al. (2003). Western Mediterranean planktonic foraminifera events and millennial climatic variability during the last 70 kyr. *Marine Micropaleontology*, 48 (1-2), 49-70.

Pinardi, N., & Masetti, E. (2000). Variability of the large scale general circulation of the Mediterranean Sea from observations and modelling: a review. Palaeogeography, Palaeoclimatology, Palaeoecology, 158, 153–173.

Pinot J.M., Tintore J., Gomis D., (1995). Multivariate analysis of the surface circulation in the Balearic Sea. *Progress in Oceanography* 36: 343–376.

Piva A., Asioli A., Trincardi F., et al. (2008). Late Holocene climate variability in the Adriatic Sea (Central Mediterranean). *The Holocene* 18: 153–67.

Pujol C., Vergnaud Grazzini C., (1995). Distribution patterns of live planktic foraminifers as related to regional hydrography and productive systems of the Mediterranean Sea. *Marine Micropaleontology* 25: 187 – 217.

Rigual-Hernández A., Sierro F.J., Bárcena M.A., Flores J.A., Heussner S., (2012). Seasonal and interannual changes of planktic foraminiferal fluxes in the Gulf of Lions (NW Mediterranean) and their implications for paleoceanographic studies: Two 12-year sediment trap records. *Deep-Sea Research* I 66, 26–40.

Rohling, E.J., Den Dulk, M., Pujol C., Vergnaud-Grazzini, C. (1995). Abrupt hydrographic change in the Alboran Sea (western Mediterranean) around 8000 yrs BP. *Deep-Sea Research* I, Vol. 42, N. 9, pp. 1609-1619.

Rohling E.J., Jorissen F.J., Vergnaud Grazzini C., et al. (1993). Northern Levantine and Adriatic planktonic foraminifera: Reconstruction of paleoenvironmental gradients, *Marine Micropaleontology* 21: 191 – 218.

Rohling E.J., Mayewski P.A., Abu-Zied R.H., et al (2001). Holocene atmosphere-ocean interactions: records from Greenland and the Aegean Sea. *Climate Dynamics* 18: 587–593.

Rohling E.J., Sprovieri M., Cane T.R., Casford J.S.L., Cooke S., Bouloubassi I., Emeis K.C., Schiebel R., Rogerson M., Hayes A., Jorissen F.J., Kroon D. (2004). Reconstructing past planktic foraminifera habitats using stable isotope data: a case history for Mediterranean Sapropel S5. Marine Micropaleontology 50:89-123.

Sánchez-López, G., Hernàndez, A., Pla-Rabes, S., Trigo, R.M., Toro, M., Granados, I., Sàez, A., Masqué, P., Pueyo, J.J., Rubio-Inglés, M.J., Giralt, S., (2016). Climate reconstruction for the last two millennia in central Iberia: The role of East Atlantic (EA), North Atlantic Oscillation (NAO) and their interplay over the Iberian Peninsula. *Quaternary Science Reviews*, 149, 135-150.

Sanvoisin R., d'Onofrio S., Lucchi R., et al. (1993). 1 Ma paleoclimatic record from the Eastern Mediterranean - MARFLUX project: first results of a micropaleontological and sedimentological investigation of a long piston core from the Calabrian Ridge. *Il Quaternario* 6:169−188.

Sbaffi L., Wezel F.C., Curzi G., et al (2004). Millennial- to centennial-scale palaeoclimate variations during Termination I and the Holocene in the central Mediterranean Sea, *Global and Planetary Change* 40: 201 – 217.

Schiebel R., Hemleben C., (2005). Modern planktic foraminifera. *Palaöntologische Zeitschrift* 79 (1), 135–148.

Schiebel R., J. Waniek A. Zeltner Alves M., (2002). Impact of the Azores Front on the distribution of planktic foraminifers, shelled gastropods, and coccolithophorids. *Deep Sea Research* part II, 49, 4035–4050.

Schilman B., Bar-Matthews M., Almogilabin A., et al (2001). Global climate instability reflected by Eastern Mediterranean marine records during the late Holocene. *Palaeogeography, Palaeoclimatology, Palaeoecology* 176: 157–176.

Schroeder K., Garcìa-Lafuente J., Josey S.A., et al (2012). Circulation of the Mediterranean Sea and its variability, in: The Climate of the Mediterranean Region, from the past to the future, edited by: Lionello, P., Elsevier Insights, Amsterdam.

Schroeder, K., Josey, S.A., Herrmann, M., Grignon, L., Gasparini, G.P., Bryden, H.L., 2010. Abrupt warming and salting of the Western Mediterranean Deep Water after 2005: Atmospheric forcings and lateral advection. Journal of Geophysical Research 115. doi:10.1029/2009JC005749

Send U., Font J., Krahmann G., et al (1999). Recent advances in observing the physical oceanography of the western Mediterranean Sea. *Progress in Oceanography* 44: 37 – 64.

Shackleton, N. J. (1967). Oxygen isotope analyses and Pleistocene temperatures reassessed. Nature,

215, 15–17.

Sicre M.A., Jalali B., Martrat B., Schmidt S., Bassetti M.A., Kallel N., (2016). Sea surface temperature variability in the North Western Mediterranean Sea (Gulf of Lions) during the Common Era. *Earth and Planetary Science Letters* vol. 456, 124-133.

Spötl C., Vennemann T.W., (2003). Continuous-flow isotope ratio mass spectrometric analysis of carbonate minerals. *Rapid Communications in Mass Spectrometry* 17, 1004–1006.

Sprovieri R., Di Stefano E., Incarbona A., et al (2003). A high-resolution of the last deglaciation in the Sicily Channel based on foraminiferal and calcareous nannofossil quantitative distribution. *Palaeogeography, Palaeoclimatology, Palaeoecology* 202, 119–42.

Sprovieri, R., Di Stefano, E., Incarbona, A., Oppo, D.W. (2006). Suborbital climate variability during Marine Isotopic Stage 5 in the central Mediterranean basin: Evidence from calcareous plankton. Quaternary Science Review, 25, 2332 – 2342, doi:10.1016/j.quascirev. 2006.01.035

Stuiver M., Reimer P. J., Bard E., Beck J. W., Burr G. S., Hughen K. A., Kromer B., McCormac G., van der Plicht J., Spurk M., (1998). INTCAL98 radiocarbon age calibration 24,000-0 cal BP. *Radiocarbon* Vol. 40, No. 3.

Taricco C., Vivaldo G., Alessio S., et al. (2015). A high-resolution $\delta^{18}O$ record and Mediterranean climate variability. *Climate of the Past* 11: 509–522.

Taricco C., Ghil M., Alessio S., et al (2009). Two millennia of climate variability in the Central Mediterranean. *Climate of the Past* 5, 171–181.

Tedesco K., Thunnel R., (2003). High resolution tropical climate record for the last 6,000 years. *Geophysical Research Letters*, vol. 30, NO. 17, 1891.

Trouet V., Esper J., Graham N.E., Baker A., Scourse J.D., Frank D.C., (2009). Persistent positive North Atlantic Oscillation mode dominated the medieval climate anomaly. *Science* 324, 78–80.

Xoplaki E., Fleitmann D., Luterbacher J., et al (2015). The Medieval Climate Anomaly and Byzantium: A review of the evidence on climatic fluctuations, economic performance and societal change. *Quaternary Science Reviews* 136: 229-252.

Figure caption:

Fig. 1 – Location map of the study area with the position of the composite core (red point). Black arrows represent surface-water circulation: NC=North Current; BC=Balearic Current. Grey arrows represent to deep-water circulation and the shadow area corresponds to the region where Western Mediterranean Deep Water (WMDW) is formed.

Fig. 2 - Distribution in time domain of planktonic foraminiferal paleoclimatic curve, $\delta^{18}O_{G.ruber}$ (this work), $\delta^{18}O_{G.bulloides}$ (Cisneros et al., 2016), planktonic foraminifera, $\Delta^{14}C$ (Stuiver et al., 1998) with the position of the climatic phases related to the composite multicore HER-MC-MR3.1A/3.3 (Balearic Bronze Age, Roman Period, Dark Age, Medieval Climate Anomaly, Little Ice Age and Industrial Period).

Fig. 3 - Comparison in time domain between North Hemisphere mean temperatures reconstruction from different authors [Moberg et al., 2005 (blue curve); Hegerl et al., 2006, 2007 (yellow curve); Mann et al., 2008 (green curve); Ljungqvist et al., 2010 (red curve)], Temperature anomaly (C°) (Pages 2k Consortium, 2013), $\delta^{18}O_{G.ruber}$ (‰ VPDB) of Menorca core (this study), $\delta^{18}O_{G.ruber}$ (‰

VPDB) of Gulf of Gaeta (Margaritelli et al., 2016), $\delta^{18}O_{G.ruber}$ (‰ VPDB) of Gulf of Salerno (Lirer et al., 2013; 2014); $\delta^{18}O_{G.ruber}$ (‰ VPDB) of Gulf of Taranto (Grauel et al., 2013), $\delta^{18}O_{G.\ sacculifer}$ (‰ VPDB) of Adriatic Sea (Piva et al., 2008), $\delta^{18}O_{G.ruber}$ (‰ VPDB) of Israel (Schilman et al., 2001), $\Delta^{14}C$ (Stuiver et al., 1998) and NAO index (black line by Olsen et al., 2012; blue line by Trouet et al., 2009). The acronym MWE corresponds to Medieval Warm Event, and MCE to Medieval Cold. The black arrows with ages represent the ages when this areas becomes part of the Roman Empire.

Tab.1 - Tie points used on both cores to make age models with their attendant errors. Uncertainties correspond to the resolution of each age model on its respective core. Also absolute dates (AMS^{14}C and biostratigraphy based on planktonic foraminiferal assemblage) are indicated. Years are expressed as Before Common Era (BCE) and Common Era (CE). For more details on age model construction, see Cisneros et al. (2016).

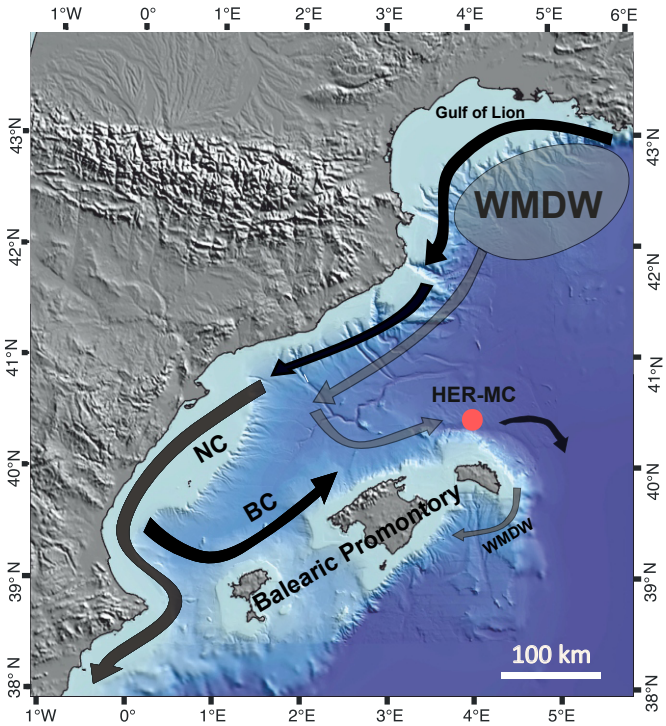
Gulf of Lion
WMDW
HER-MC
NC
BC
Balearic Promontory
WMDW
100 km
1°W
0°
1°E
2°E
3°E
4°E
5°E
6°E
43°N
42°N
41°N
40°N
39°N
38°N

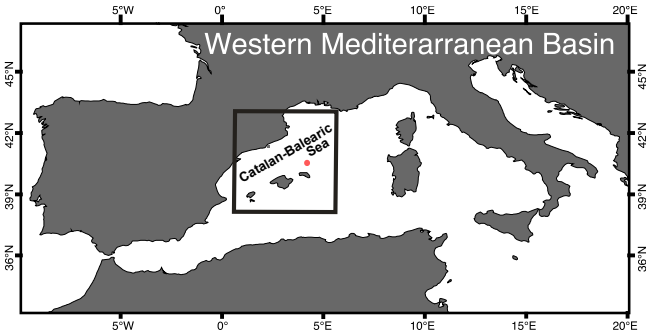
Western Mediterarranean Basin
Catalan-Balearic Sea
5°W
0°
5°E
10°E
15°E
20°E
45°N
42°N
39°N
36°N

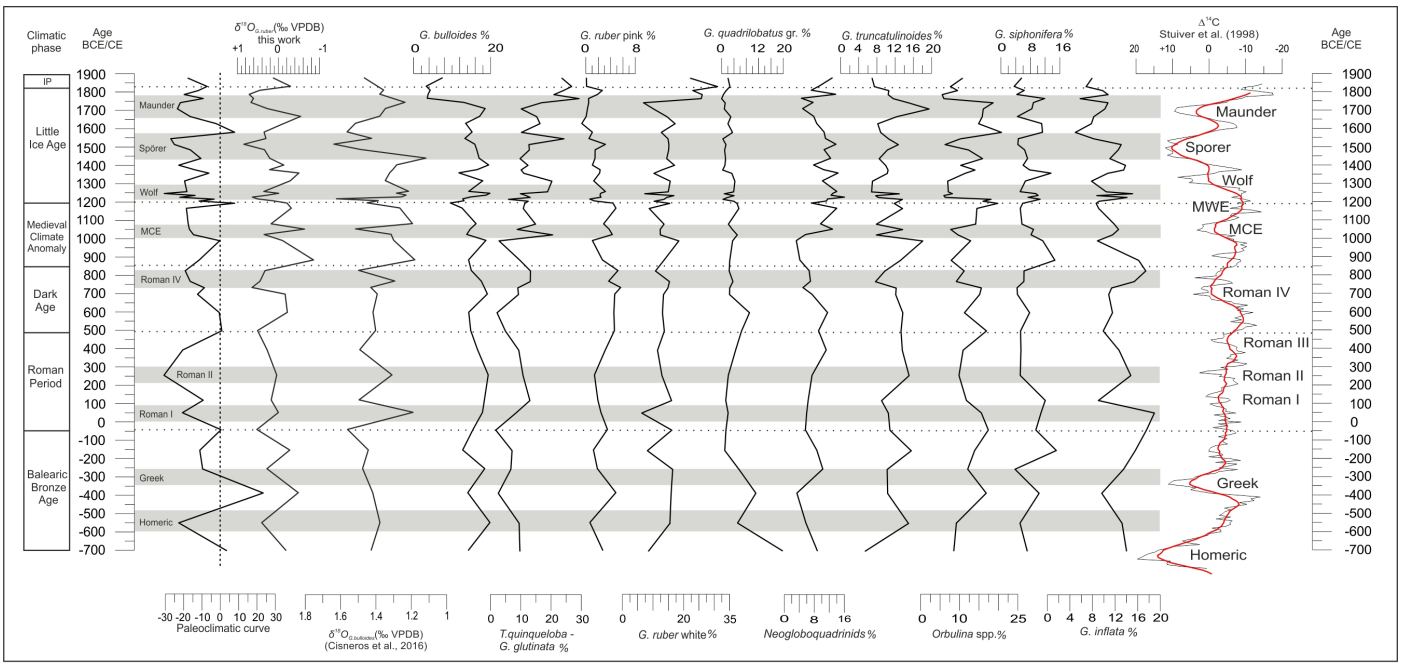
Climatic phase
Age BCE/CE
IP
Little Ice Age
Medieval Climate Anomaly
Dark Age
Roman Period
Balearic Bronze Age
Maunder
Spörer
Wolf
MCE
Roman IV
Roman II
Roman I
Greek
Homeric
this work
G. bulloides %
G. ruber pink %
G. quadrilobatus gr. %
G. truncatulinoides %
G. siphonifera %
Stuiver et al. (1998)
MWE
Roman III
Paleoclimatic curve
(Cisneros et al., 2016)
T.quinqueloba - G. glutinata %
G. ruber white %
Neogloboquadrinids %
Orbulina spp. %
G. inflata %

Fig.2

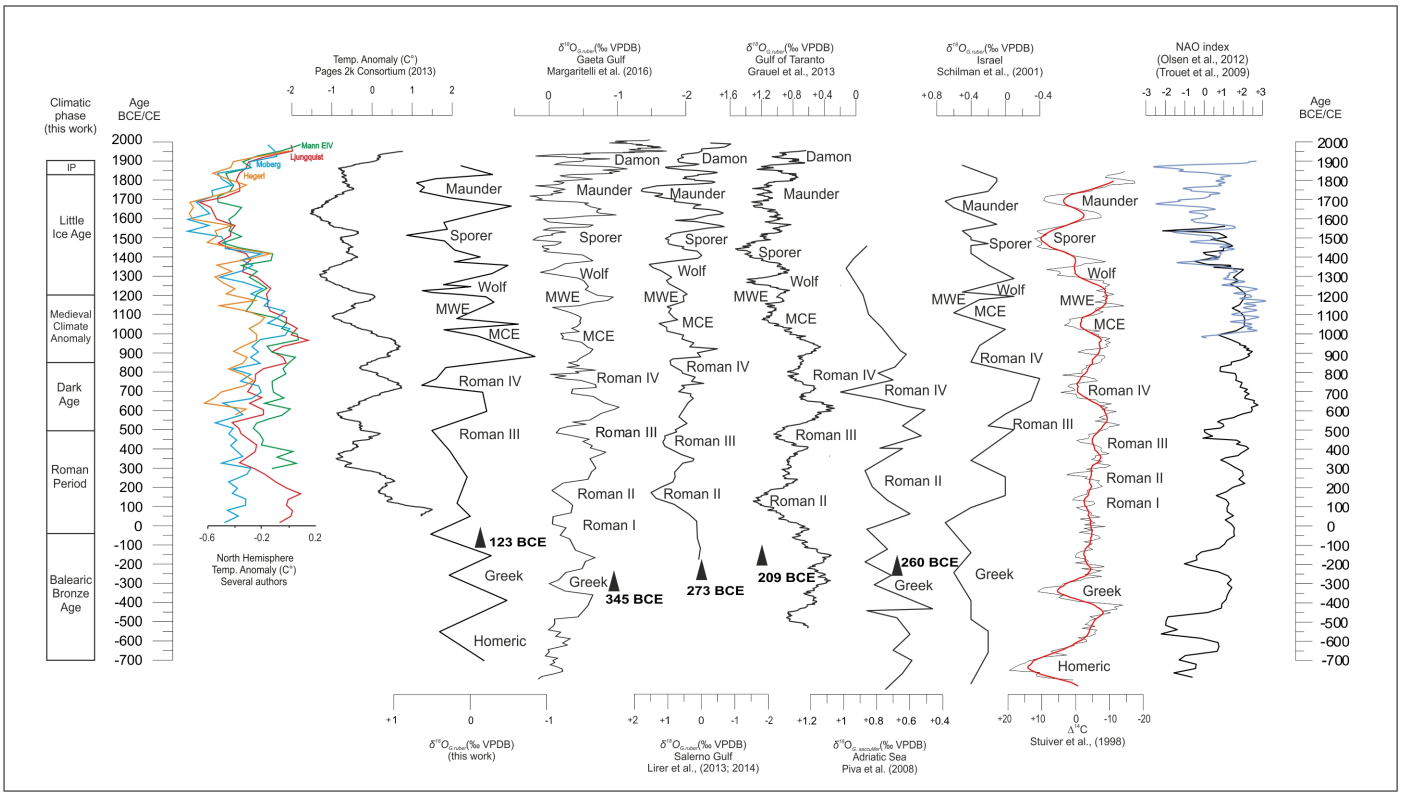
Climatic phase (this work)
Age BCE/CE
IP
Little Ice Age
Medieval Climate Anomaly
Dark Age
Roman Period
Balearic Bronze Age
Mann EIV
Ljungqvist
Moberg
Hegerl
North Hemisphere Temp. Anomaly (C°) Several authors
Temp. Anomaly (C°) Pages 2k Consortium (2013)
Gaeta Gulf Margaritelli et al. (2016)
Gulf of Taranto Grauel et al., 2013
Israel Schilman et al., (2001)
NAO index (Olsen et al., 2012) (Trouet et al., 2009)
Maunder
Sporer
Wolf
MWE
MCE
Damon
Roman IV
Roman III
Roman II
Roman I
Greek
Homeric
123 BCE
345 BCE
273 BCE
209 BCE
260 BCE
(this work)
Salerno Gulf Lirer et al., (2013; 2014)
Adriatic Sea Piva et al. (2008)
Stuiver et al., (1998)

Fig.3

Core	Composite depth (cm)	Method	Ages (years BCE/CE)		Age-uncertainties interval (years BCE/CE)	
MR3.1A	5-5.5	Mg/Ca	1627	CE	1545-1665	CE
	6.5-7		1400	CE	1350-1484	CE
	10-10.5		1050	CE	1021-1165	CE
	12.5-13		766	CE	597-824	CE
	13-13.5	Mn ICP-MS	597	CE	497-766	CE
	13.5-14	Mg/Ca	497	CE	433-597	CE
	15-16	Mn ICP-MS	254	CE	184-390	CE
	21-22	Mg/Ca	133	BCE	170 BCE-25	CE
	22-23	Mn ICP-MS	170	BCE	207 -133	BCE
	24-25		551	BCE	625-207	BCE
	26-27	Mg/Ca	702	BCE	779-625	BCE
MR3.3	0.5-1	*G. truncatulinoides* peak	1708	CE	1708-1728	CE
	3.5-4	AMS14C	1484	CE	1383-1484	CE
	6.5-7		1256	CE	1063-1256	CE
	12-12.5		989	CE	9111085	CE
	16-17		497	CE	438-621	CE
	20-21		50	CE	88 BCE-107	CE
	24-25		388	BCE	388-214	BCE
	26-27	*G.quadrilobatus* top acme	702	BCE	798-702	BCE

Samples	Age (CE/BCE) Cisneros et al. (2016)	$\delta^{18}O$ *G. ruber vs* VPDB	*G.bulloides*	*G.glutinata*	*G.ruber* pink	*G.ruber* white	*G.sacculifer*	*G.quadrilobatus*	*G.inflata*	*T.quinqueloba*	*G.siphoniphera*
HEMC-MR 3.1	1875.0	0.12	32	82	5	96	1	8	34	20	24
HEMC-MR 3.1	1830.0	-0.29	11	61	4	104		9	23	29	12
HEMC-MR 3.1	1808.0	0.46	15	44	13	80	1	4	34	40	22
HEMC-MR 3.1	1786.0	0.71	14	64	11	97		2	40	14	16
HEMC-MR 3.1	1764.0	0.61	14	80	6	102			23	36	47
HEMC-MR 3.3	1741.5	0.67	34	21	4	18		3	28	23	23
HEMC-MR 3.3	1708.0	0.27	42	13	3	23		2	23	10	19
HEMC-MR 3.3	1665.5	-0.54	46	13	3	39	1	7	22	28	12
HEMC-MR 3.3	1627.5	-0.13	33	9	1	42	3	2	19	31	27
HEMC-MR 3.3	1580.0	0.35	43	11	6	36	2	8	14	18	32
HEMC-MR 3.3	1545.0	0.30	34	14	4	38		1	21	48	12
HEMC-MR 3.3	1513.5	0.84	45	21	12	43	4		37	15	13
HEMC-MR 3.3	1484.0	0.34	51	24	8	47	2	1	39	16	20
HEMC-MR 3.3	1437.0	0.21	40	12	6	34		3	26	11	17
HEMC-MR 3.3	1400.3	-0.13	55	23	6	48		3	39	12	17
HEMC-MR 3.3	1375.0	0.21	49	13	10	38		1	40	17	23
HEMC-MR 3.3	1357.0	-0.50	32	19	9	28	1	8	29	11	37
HEMC-MR 3.3	1314.0	-0.29	46	14	6	40	2	9	20	38	17
HEMC-MR 3.3	1256.0	0.36	44	17	13	46		12	32	41	16
HEMC-MR 3.3	1245.8	-0.01	46	10	8	17		2	35	13	22
HEMC-MR 3.3	1235.5	0.28	56	18	10	50	1	11	26	17	30
HEMC-MR 3.3	1225.3	0.63	46	21	11	45	1	5	44	20	23
HEMC-MR 3.3	1215.0	0.50	30	2	4	32		1	28	12	25
HEMC-MR 3.3	1204.8	0.11	43	10	8	34		13	30	31	28
HEMC-MR 3.3	1192.9	-0.21	21	7	12	34	2	9	19	18	13
HEMC-MR 3.3	1165.0	-0.31	36	22	17	25		16	26	9	15
HEMC-MR 3.3	1079.6	0.18	37	13	9	31	1	4	27	21	13
HEMC-MR 3.3	1050.8	-0.63	55	9	18	46	1	12	47	24	33
HEMC-MR 3.3	1021.1	0.35	49	31	19	44		18	41	42	29
HEMC-MR 3.3	988.6	-0.09	53	4	6	52	7	3	25	4	32
HEMC-MR 3.3	882.2	-0.85	38	6	10	36	2	5	43	20	39
HEMC-MR 3.3	824.4	0.33	43	12	18	31	1	6	50	26	18
HEMC-MR 3.3	766.6	0.45	48	14	13	42	3	7	42	22	17
HEMC-MR 3.3	732.0	0.64	63	23	23	51	3	6	39	8	15
HEMC-MR 3.3	696.0	-0.16	60	17	18	42	8		34	12	14
HEMC-MR 3.3	596.5	-0.22	46	3	18	42	4	25	37	4	25
HEMC-MR 3.3	497.0	0.51	39	13	15	36	7	10	26		14
HEMC-MR 3.3	392.1	0.28	55	15	14	38		15	42	16	18
HEMC-MR 3.3	254.4	0.04	63	26	8	42		7	48	9	17
HEMC-MR 3.3	118.0	0.18	55	35	9	48		4	27	4	36
HEMC-MR 3.3	49.9	0.00	51	18	10	18		6	54	6	31
HEMC-MR 3.3	-43.0	0.52	44	5	13	46	4		50		27
HEMC-MR 3.3	-155.0	-0.27	50	12	9	32	1	3	61	16	59
HEMC-MR 3.3	-257.0	0.28	63	8	10	56		19	46	15	13
HEMC-MR 3.3	-388.0	-0.48	38	7	16	43	6	24	26		28
HEMC-MR 3.3	-551.0	0.41	69	8	6	54		18	46	25	18
HEMC-MR 3.3	-702.0	-0.18	60	19	16	36	35	48	59	22	30

Orbulina spp.	*N.pachyderma* sx	*N.pachyderma* dx	*G.truncatulinoides* dx	*G.truncatulinoides* sx	*N.dutertrei*	*Clavatorella* spp.	TOT planctonici
42		55	2	30			399
26		31		25		2	324
33		25		37			333
21		51		39		3	358
24		18		46			382
48		8		39	12		227
36		4		44	7		184
42		6		33	15	1	222
36		5		20	16		211
58		9		25	21		240
26		6		27	22	2	221
18		7		36	32		238
38		5		32	28		260
37		13		20	16		195
29		10		28	12		227
41		4		31	27	2	247
31		12		28	27		240
18		6		18	20	2	210
22		10		21	33		263
19		5		30	25		186
18		21		23	16		241
20		17		26	33		266
42		8		32	19		205
52		17		42	20		285
43		5		26	11		199
41		35		39	5		250
32		14		18	8		191
29		16		51	32		318
34		5		28	15		306
36				51	9	3	229
21		2		35	9		228
32		2		28	17	3	244
25		5		21	14		225
53		6		42	11		280
47		7		38	16		253
36		18		44	19		275
44		11		35	13		224
36		16		45	21		276
32		11		49	13		262
35		12		27	7		244
44		9		30	8		234
49		8		31	8		241
54		2		61	32		342
41		5		35	30		278
45				28	9		232
32		7		52	13		279
36		4		23	33		361